RSC Advances

PAPER

View Article Online
View Journal | View Issue

Cite this: *RSC Adv.*, 2024, **14**, 3070

Dual stimuli-responsive polymeric nanoparticles combining soluplus and chitosan for enhanced breast cancer targeting

Shrouq Twal,[ab] Nisrein Jaber,[c] Mayyas Al-Remawi,*[a] Islam Hamad,[b] Faisal Al-Akayleh [a] and Walhan Alshaer *[d]

A dual stimuli-responsive nanocarrier was developed from smart biocompatible chitosan and soluplus graft copolymers. The copolymerization was investigated by differential scanning calorimetry (DSC), thermogravimetric analysis (TGA), and Fourier transform infrared (FTIR). The optimized chitosan-soluplus nanoparticles (CS-SP NPs) were further used for the encapsulation of a poorly water-soluble anticancer drug. Tamoxifen citrate (TC) was used as the model drug and it was loaded in CS-SP NPs. TC CS-SP NPs were characterized in terms of particle size, zeta potential, polydispersity, morphology, encapsulation efficiency, and physical stability. The nanoparticles showed homogenous spherical features with a size around 94 nm, a slightly positive zeta potential, and an encapsulation efficiency around 96.66%. Dynamic light scattering (DLS), *in vitro* drug release, and cytotoxicity confirmed that the created nanosystem is smart and exhibits pH and temperature-responsive behavior. *In vitro* cellular uptake was evaluated by flow cytometry and confocal microscopy. The nanoparticles revealed a triggered increase in size upon reaching the lower critical solution temperature of SP, with 70% of drug release at acidic pH and 40 °C within the first hour and a 3.5-fold increase in cytotoxicity against MCF7 cells incubated at 40 °C. The cellular uptake study manifested that the prepared nanoparticles succeeded in delivering drug molecules to MCF7 and MDA-MB-231 cells. In summary, the distinctive characteristics provided by these novel CS-SP NPs result in a promising nano-platform for effective drug delivery in cancer treatment.

Received 25th November 2023
Accepted 13th January 2024

DOI: 10.1039/d3ra08074a

rsc.li/rsc-advances

1 Introduction

Breast cancer (BC) is the second most prevalent cancer worldwide, after lung cancer. About 20% of cancer patients have BC, and it is the leading cause of mortality among women.[1] Fortunately, non-metastatic BC is treatable in approximately 70–80% of instances, particularly in the disease's early stages.[2] Tamoxifen (TC) (Fig. 1A) is a gold standard in BC treatment as it is one of the most popular selective estrogen receptor modulators (SERMs).[3] It is a hydrophobic, potent anticancer drug, approved by FDA for the management of BC in both females and males.[4] Biopharmaceutics Classification System (BCS) classifies TC as a class II drug characterized by low water solubility and poor oral bioavailability in the range of 20–30%.[5]

Poor bioavailability, severe side effects, cytotoxicity and non-specific action of anticancer drugs are the major challenges in developing their delivery systems.[6,7] A promising approach to solve these challenges is applying polymeric nanocarriers as reservoirs to anticancer pharmaceutical ingredients.[8–10] Nanoparticles (NPs) as drug carrier can encapsulate hydrophobic compounds, thereby improving their solubility, biocompatibility, and retention time in tumor permeable vasculature,[11,12] thereby releasing the drug in a controlled manner.[13] In addition, NPs can improve intracellular penetration and specificity towards a specified target by being attached to targeting ligands for therapeutic or diagnostic reasons.[14] The Enhanced Permeability and Retention (EPR) effect is a phenomenon in which NPs tend to accumulate selectively in tumor tissues through passive targeting.[15,16] Endothelial cells in tumor vessels are not closely packed and instead have a vast gap between them that is about 100–800 nm larger than in normal physiological conditions. Furthermore, because lymphatic drainage is impaired in tumor tissues, these nanocarriers can remain in tumor for days or weeks, facilitating adequate drug release and accumulation.[17] Micelles are nanometer-sized vesicles with a hydrodynamic diameter range from 1 to 200 nm produced by the self-assembly of amphiphilic polymers.[18,19] This form of NPs comprises an inner hydrophobic core and an outer hydrophilic shell. A modification of the outer shell of nanomicelles can improve their properties, for instance by enhancing targeting.[20,21] Polymeric micelles (PMs) can be used to deliver a range of pharmaceutical

[a]*Faculty of Pharmacy and Medical Sciences, University of Petra, Amman 1196, Jordan. E-mail: malremawi@uop.edu.jo; Tel: (+962) 797683190*

[b]*Faculty of Health Sciences, American University of Madaba, Amman 11821, Jordan*

[c]*Faculty of Pharmacy, Al Zaytoonah University of Jordan, Amman 11733, Jordan*

[d]*Cell Therapy Center, The University of Jordan, Amman 11942, Jordan. E-mail: walhan.alshaer@ju.edu.jo; Tel: (+962) 790823678*

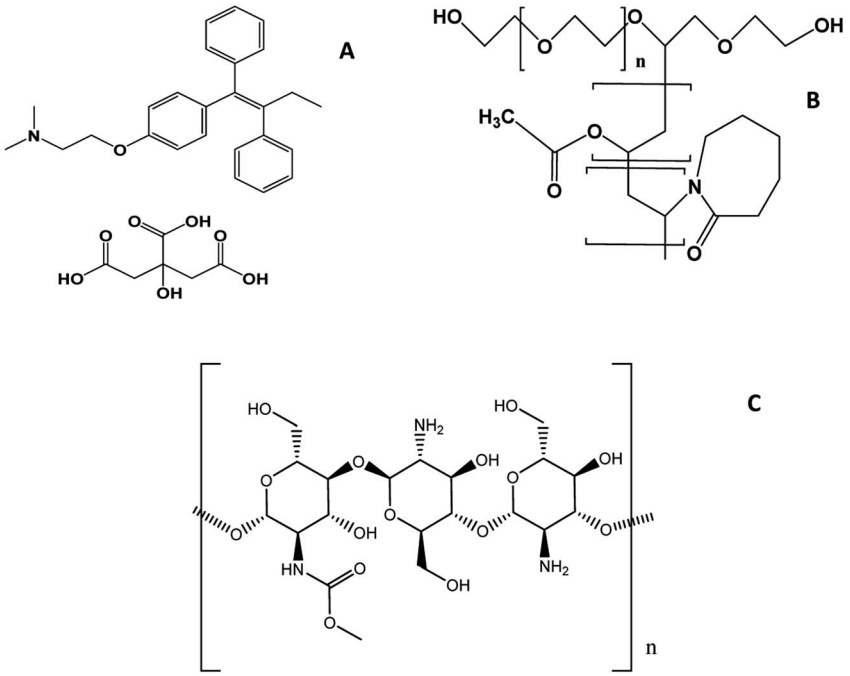

Fig. 1 Chemical structure of (A): tamoxifen citrate,[35] (B): soluplus[36] and (C): chitosan.[37]

active ingredients at a controlled rate due to their simple preparation methods, biocompatibility, and highly potential to encapsulate poorly soluble and lipophilic molecules.[6] As recorded, PMs can be applicable to use for the delivery of anticancer drugs.[22] Particularly, encapsulating hydrophobic anticancer drugs inside PMs can increase their aqueous solubility by a factor of up to 500, thus increasing their biological behavior and enhancing accumulation in the targeted site with fewer side effects on normal tissues.[3,23] Advances in polymer chemistry produce intelligent polymeric systems with greater regulation of the physicochemical characteristics, which is crucial for the precise delivery of anticancer drugs. Intelligent or environmentally-stimuli polymers are polymers that undergo structural modifications when triggered by chemical or physical stimuli.[24] Temperature, light, shear, and magnetic field are among the physical stimuli used, whereas pH, redox, enzymes, and hypoxia are all known as chemical stimuli. These triggers can be intrinsic and come from the biological environment of the body such as changes in temperature, pH, enzymes, redox, and hypoxia or extrinsic exposure of triggers such as changes in temperature, magnetic field, and light.[25] Functionalized polymeric NPs such as PMs with stimuli-responsive characteristics would allow for regulation of the distribution and release of the drug at the disease site.[26,27]

Soluplus (SP) (Fig. 1B), is a thermos-responsive graft copolymer, composed of polyethylene glycol backbone as the hydrophilic moiety and vinyl caprolactam/vinyl acetate side chain as the hydrophobic part. Its biocompatible profile and

Table 1 Physical characterization of different molar ratios of CS-SP NPs, the NPs prepared at optimal CS to SP molar ratios (1 : 1) (mean ± SD, $n = 3$)

Sample	Average diameter (nm)	PdI	Zeta potential (mV)
CS	593.83 ± 28.21	0.75 ± 0.11	0.4 ± 4.1
CS : GA	365.61 ± 26.33	0.88 ± 0.17	12.3 ± 3.2
SP	77.23 ± 1.19	0.07 ± 0.04	−4.4 ± 5.4
SP : GA	69.34 ± 1.41	0.05 ± 0.03	−8.8 ± 6.1
CS:SP NPs (cross-linked with GA)			
100 : 1	128.09 ± 3.61	0.34 ± 0.04	12.8 ± 4.6
10 : 1	93.09 ± 1.88	0.09 ± 0.05	7.4 ± 4.7
2 : 1	201.87 ± 4.86	0.25 ± 0.04	1.6 ± 5.1
1 : 1	86.92 ± 1.61	0.10 ± 0.05	2.4 ± 1.0
1 : 2	101.15 ± 2.01	0.10 ± 0.05	−2.5 ± 3.3
Drug loaded CS-SP NPs			
TC NPs (optimal)	94.17 ± 4.01	0.27 ± 0.01	9.3 ± 0.2

amphiphilic nature have led to its extensive use as a solubilizer for numerous poorly water soluble drugs.[28–34]

SP is a type of temperature responsive polymer that responds to temperature changes and undergoes phase transition at the lower critical solution temperature (LCST). Herein, at temperatures below the LCST, It's macromolecules become hydrophilic, while at temperatures above the LCST, these macromolecules are hydrophobic.[26,38] SP is capable of forming nanometer scale micelles in aqueous media with a small hydrodynamic diameter and narrow particle size distribution, it has a critical micelle concentration (CMC) of 7.6 mg L^{-1}. In this regard, micelles generated *via* SP with low CMC are less prone to deform when facing the infinite diluting effects *in vivo*.[39,40] SP exhibited a promising ability to create stable and small self-assembled micellar systems composed of a hydrophobic inner core and an outer hydrophilic shell with sufficient drug loading and colloidal stability, hence enhancing therapeutic effectiveness of loaded compounds.[41]

pH-responsive polymers are types of smart polymers that undergo substantial alterations in their physicochemical characteristics when exposed to a minor alteration in pH. They have ionizable functional groups that can either receive or liberate protons in response to pH changes, leading to a switch between a charged and neutral state of the polymer.[24,42] The extracellular tumor pH is more acidic than the pH of healthy tissues and blood because of the rapid proliferation of tumor that induces glycolysis, which is a distinguishing feature of cancer cells aids in controlled drug release.[43] The pH range of the tumor is between 5.8 and 7.8, with a mean of 6.0. Nonetheless, intracellular pH can be reduced. Lysosome pH values vary from 4.0 to 5.0, while endosome pH values range from 5.0 to 6.0. The pH-responsive PMs are anticipated to be able to promote cellular uptake, anticancer efficacy, and release pharmacological payloads in a well-controlled way through pH-triggered structural transformation in the acidic microenvironment of tumor cells.[44–46] Chitosan (CS) (Fig. 1C) has the greatest promise for use in biomedical applications and drug delivery, as it has exceptional versatile biodegradability and biocompatibility, amenability to chemical modification most commonly using amino groups ($-NH_2$) and minimal immunogenicity.[47–51] It is commonly used as a coating or in the matrix of NPs for developing DDSs, including proteins, antibodies, DNA, hormones, medicines, and even natural compounds.[52,53] Considering the hydrophilic nature of CS and to avoid a premature drug release, cross linking agents like glutaraldehyde (GA) have been widely employed to enhance the properties of CS.[54] Henceforth, the hydrophobically modified CS micelles triggered by more than one stimulus is an alternative strategy for enhancing the efficacy and rate of drug delivery.[55]

In comparison to other stimuli, temperature and pH, two of the most frequently used in the development of smart DDSs by means of nanotechnology to deliver drug molecules. As a number of disorders, including cancer, diabetes, and others, have been linked to changes in physiological temperature and pH.[56,57] NPs have an intelligent release profile through releasing their payloads in response to both decreased pH as well as raised temperature. Two or more different polymeric blocks can chemically co-polymerized to produce a dual responsive nanocarriers with higher therapeutic efficacy.[58]

The objective of this study is to develop a highly efficient and responsive drug delivery system for TC, a widely used anti-breast cancer drug. This research aims to join the advantages of polymeric nanocarriers, specifically polymeric micelles (PMs), with an emphasis on their responsive behavior to temperature and pH changes. By combining the thermos-responsive properties of Soluplus (SP) and the pH-responsive characteristics of chitosan (CS), a novel intelligent drug delivery system capable of precise drug distribution and controlled release is developed. The study also investigates the potential benefits of dual responsiveness to both temperature and pH changes in enhancing the therapeutic efficacy of TC delivery, particularly in the context of breast cancer treatment.

2 Materials and methods

2.1 Materials

Chitosan (CS) (low molecular weight poly *N*-acetyl glucosamine, viscosity average MWt was around 10 kDa, with Degree of deacetylation, DDA > 98%) was a gift from Jordanian Pharmaceutical Manufacturing Co., PLC, Jordan. Tamoxifen citrate was a gift from RAM Pharmaceutical Industries Co., Jordan. Soluplus® (SP) (triblock graft copolymer comprising polyvinyl caprolactam (57%), polyvinyl acetate (30%), and polyethylene glycol (13%) having a molecular weight ranging from 90 to 140 kDa, and with HLB value ~14.0) was obtained from BASF, Germany. Glutaraldehyde was purchased from Sigma-Aldrich, USA. All other chemicals and reagents were of analytical grade and ultrapure water was used throughout the work.

2.2 Methods

2.2.1 Preparation of nanoparticles. The experimental procedure involved the utilization of glutaraldehyde (GA) as a chemical cross-linking agent to enhance the stability of the micelles and reduce the initial burst release, following established protocols.[45,59] In a summarized procedure, CS was dissolved in a solution of 1% acetic acid to achieve a concentration of 0.01 g mL^{-1} and the solution pH was around 5.9. Simultaneously, SP was dispersed in distilled water at a concentration of 1% w/v. The reaction began by adding a commercial 25% w/v aqueous GA solution as a cross-linker to the CS solution. Immediately, the SP dispersion was introduced into the CS/GA mixture at various CS : SP molar ratios (100 : 1, 10 : 1, 2 : 1, 1 : 1, 1 : 2), with continuous stirring at room temperature to facilitate the formation of CS-SP nanoparticles. Following a one-week incubation period, any unreacted GA and residual glacial acetic acid were removed by subjecting the mixture to dialysis against 0.5 L of distilled water. Dialysis was carried out using a cellulose dialysis membrane (Frey Scientific, USA) for a duration of 24 hours. Water used for dialysis was changed three times during the 24 hours period.

2.2.2 Preparation of drug loaded nanoparticles. The preparation of TC loaded nanoparticles was achieved according to the method performed by[60] with slight modification. Briefly, TC

was firstly dissolved in ethanol. The concentration of TC in ethanol was 1.08 mM. CS-SP NPs with a 1 : 1 molar ratio were prepared previously; TC solution was added dropwise to CS-SP NPs with continuous stirring for 30 min, and then ethanol was evaporated under a fume hood at room temperature to obtain TC loaded CS-SP NPs (TC-CS-SP NPs). The container was protected from light, as TC is a light-sensitive drug.

2.2.3 Characterization of nanoparticles

2.2.3.1 DLS studies. Hydrodynamic diameter, polydispersity index (PdI), and zeta potential were analyzed by dynamic light scattering (DLS) using (Zetasizer Nano ZS, Malvern Instruments, Worcestershire, UK) equipped with Zetasizer software for data analysis. DLS measurement for each sample was conducted at 25 °C with a 173° scattering angle and lasted for 60 s. The analyses were carried out in triplicate; data is expressed as mean ± SD.

2.2.3.2 Effect of temperature and pH on particle size. DLS experiment was performed according to the method published by[61] with slight modifications in order to investigate the influence of temperature on hydrodynamic diameter of SP, SP : GA, CS, CS : GA, and different molar ratios of CS-SP NPs (100 : 1, 10 : 1, 2 : 1, 1 : 1, 1 : 2). The experiment was conducted with an automatic program over a temperature range of 20 to 65 °C after equilibration of the samples for 2 minutes at each temperature and increasing the temperature by 5 °C. At each temperature point, each sample was measured three times.

Further DLS experiment was conducted to investigate the effect of different ranges of pH on hydrodynamic diameter, PdI, and zeta potential for different molar ratios of CS-SP NPs. The pH of CS-SP NPs was adjusted to a desired value with 1 M HCL and 1 M NaOH.[62]

2.2.3.3 High performance liquid chromatography (HPLC) studies. HPLC studies were used to determine TC content. HPLC system consists of HPLC (Finnigan Surveyor) (Thermo Electron Corporation, San Jose, CA, USA), pump (solvent delivery systems pump) (LC Pump plus) equipped with autosampler (Autosampler Plus) and variable wavelength UV detector (UV-VIS Plus Detector), data were analyzed using ChromQuest software 4.2.34.

TC was determined according to the method previously described by[63] with slight modifications. The sample was injected into InertSustain (GL Sciences) C-8 column (4.6 × 150 mm, 5 μm). Freshly prepared mobile phase composed of methanol and phosphate buffer pH 7.4 (9 : 1) was filtered through a 0.45 μm nylon membrane filter and then sonicated to degas before use. The flow rate was 1 mL min^{-1}, the injection volume was 50 μL, and the temperature was 25 °C. The detection was conducted using a UV-Vis detector at a wavelength of 277 nm. The retention time of TC was approximately 4.2 min. The calibration curve was prepared from a stock solution of TC (0.9 mg mL^{-1}) and then diluted with the mobile phase to different known concentrations in the range of 10–100 μg mL^{-1}. The linear correlation coefficient was around 0.998.

2.2.3.4 Determination of entrapment efficiency and loading capacity. The entrapment efficiency (EE) and drug loading (DL) of TC into CS-SP NPs were determined by centrifugation.[64] Briefly, TC-CS-SP NPs were centrifuged at 14 000 rpm for 15 min, at 25 °C (Heraeus Fresco 21 Centrifuge, Thermo scientific). After centrifugation, the supernatant was collected, diluted with methanol and phosphate buffer pH 7.4 (9 : 1), and analyzed for the encapsulated TC concentration. The concentration of TC was determined before and after centrifugation by the HPLC method mentioned previously. The EE and DL were Amount of added drug and polymer

$$\mathrm{EE}(\%) = \frac{\text{Amount of drug after centrifugation}}{\text{Amount of drug added}} \times 100 \quad (1)$$

$$\mathrm{DL}(\%) = \frac{\text{Amount of drug after centrifugation}}{\text{Amount of added drug and polymer}} \times 100 \quad (2)$$

2.2.3.5 Morphology study. The morphological characterization of CS-SP NPs and TC-CS-SP NPs was investigated using scanning transmission electron microscopy (STEM) (Versa 3D, FEL, Netherlands) operated at 30 kV. Before conducting the analyses, samples were diluted in water and deposited onto a carbon-coated copper grid with a 100-mesh opening size. To create a thin film, most of the sample was wiped with filter paper. After the formulation was adhered, 5 μL of phosphotungstic acid solution (1% w/v in sterile water) was placed onto the grid as a negative staining medium, and the surplus solution was blotted away using filter paper. Samples were kept dry at room temperature, and then visualized under the electron microscope.[65]

2.2.3.6 Fourier transform infrared (FTIR) spectroscopy. Infrared spectra of CS, SP, CS-SP physical mixture, CS-SP NPs, TC-CS-SP physical mixture, and TC-CS-SP NPs were recorded with FTIR device (FTIR-7600 Agilent Technologies Inc., Fourier Transform Infrared Spectrophotometer, Danbury, CT, USA) using the potassium bromide (KBr) disk pellet technique. First, sample powder was mixed with KBr, with a 1 mg sample per 300 mg of KBr. Then the prepared sample was compressed on a hydraulic press at 3000 psi to make a transparent pellet.[54] The spectra were scanned at a resolution of 1 cm^{-1} and scanning region wavelength 400–4000 cm^{-1}. The analysis aimed to corroborate the CS-SP cross linking with GA.

2.2.3.7 Differential scanning calorimetry (DSC) analysis. DSC analysis was conducted to examine the thermal behavior of various samples, including CS, SP, TC, CS-SP physical mixture, CS-SP NPs, TC-CS-SP physical mixture, and TC-CS-SP NPs. The analysis aimed to investigate the chemical cross-linking of CS and SP in CS-SP NPs and understand the thermal properties of the different samples. The DSC analysis was performed using (Mettler-Toledo DSC1, GmbH, Germany) equipped with a cooling system was used with the following instrument conditions: approximately 3 mg of each sample was placed in a 40 μL hermetically sealed aluminum pan and then heated from 25 to 300 °C at a scanning rate of 10 °C min^{-1} under a constant flow of nitrogen gas (5.0 mL min^{-1}). An empty aluminum pan was placed in DSC device as a ref. [66].

2.2.3.8 Thermogravimetric analysis (TGA). TGA was performed to evaluate thermal properties of CS, SP, TC, CS-SP physical mixture, CS-SP NPs, TC-CS-SP physical mixture, and TC-CS-SP NPs. TGA curves were monitored using (Mettler

Toledo TGA/DSC 2-star system, Switzerland). Approximately 3 mg of each sample was placed in a 70 μL alumina crucible and then heated from 30 to 500 °C at a heating rate of 10 °C min^{-1} under a constant flow of nitrogen gas (50 mL min^{-1}).[67]

2.2.4 *In vitro* drug release study. To confirm the hypothesis that TC-CS-SP NPs are pH and temperature stimuli-responsive nanoparticles, the release of TC was monitored in different pH and temperature conditions.[68,69] In this regard, the drug release profile of TC from TC-CS-SP NPs was evaluated using the dialysis membrane method (cellulose membrane, Frey scientific, USA). The release was determined in two different pH dissolution media prepared from Tris-HCL buffer and at two temperatures. In brief, 9 mL of TC-CS-SP NPs were dialyzed against 100 mL of each buffer (pH 6 or pH 7.4) and gently shaken in a shaking water bath (SB-12L shaking water bath, Benchmark, USA) at 100 rpm. The temperature was set to 37 ± 2 °C and then the same procedure was performed again at 40 ± 2 °C. At predetermined time points (1, 2, 3, 4, 6, 24 and 48 h), aliquots of 1 mL of the release medium were withdrawn and replaced with the same volume of the dissolution medium to maintain sink condition. The cumulative amount of TC released from NPs in the dissolution media at each time interval was quantified by HPLC technique.

2.2.5 Determination of drug stability. The stability analysis of TC-CS-SP NPs regarding hydrodynamic diameter, PdI (Polydispersity Index), and zeta potential was conducted after incubation in three different media, including phosphate buffer at pH 6 or pH 7.4. The measurements were performed using a Pro-Malvern Zetasizer instrument and analyzed using ZS XPLORER software.

The ratio between NPs and incubation media was 1 : 1 v/v. TC-CS-SP NPs were placed in phosphate buffer (pH 6 or pH 7.4) and were incubated at 4 °C and 37 °C. At a designated time, interval up to 7 days, 100 μL aliquot of each sample was withdrawn and diluted up to 1 mL with nuclease-free water before being analyzed by DLS. The analyses were performed in triplicate; data is expressed as mean ± SD.

2.2.6 Cellular studies

2.2.6.1 Cell culture. Human dermal fibroblast cell line (HDF), human breast cancer cell lines MCF7 (ER+) and MDA-MB-231 (ER-) were obtained from the Cell Therapy Center (the University of Jordan, Amman, Jordan). HDF cell line was cultured in Dulbecco's Modified Eagle Medium, human breast cancer cell line MDA-MB-231 was cultured in Minimum Essential Medium while breast cancer cell line MCF7 was cultured in RPMI 1640 Medium. Cultured medium supplemented with 10% (v/v) fetal bovine serum (FBS), 100 mg mL^{-1} streptomycin, 100 U mL^{-1} penicillin, and 2 mM L-Glutamine. The cells were maintained at 37 °C under a humidified atmosphere of 5% CO_2 incubator (Memmert, Germany). The cells were passaged approximately every 3–4 days when reaching 90% confluence, by gentle trypsinization using 0.05% (w/v) trypsin.

2.2.6.2 Cell viability assay. Cell viability was evaluated using the calorimetric MTT assay. Each experiment was performed in triplicate. Cells were seeded in 96-well plates at (8×10^3 cells per well) in the case of HDF and at (9×10^3 cells per well) in the cases of MCF7 and MDA-MB-231 and cultured for 24 h. After which, the cells were incubated with free TC, blank CS-SP NPs, or TC-CS-SP NPs at different concentrations at 37 °C and once again at 40 °C (5 min per 24 h).[70] In this instance, the elevated temperature was adjusted by raising the temperature of the incubator. For the negative control, untreated cells were incubated with the complete culture medium. After 72 h of incubation at 37 °C, treatments were removed from the wells, followed by adding 15 μL of 3-(4,5-dimethyl-2-thiazolyl)-2,5-diphenyltetrazolium bromide (MTT) solution and 100 μL of the medium to each well, and the cells were incubated at 37 °C for further 3 h. Then, the medium and MTT salt were removed and replaced with 50 μL of dimethyl sulfoxide (DMSO) to dissolve the insoluble formazan. Absorbance values were measured at a wavelength of 570 nm using Glomax microplate reader (Promega, USA). Results on relative cell viability were presented as the percentage of surviving cells in relation to untreated cells.

2.2.6.3 Cellular uptake study. To visualize TC-CS-SP NPs for cellular uptake studies, the fluorescent dye coumarin-6 was used to label TC-CS-SP NPs by co-encapsulating of coumarin-6 (100 μg per 50 mg polymer) with TC in the organic phase and then added to CS-SP NPs.[71]

MCF7, MDA-MB-231, and HDF (1×10^5 cells per well) were seeded in twelve-well plates. After being cultured for 24 h, the cells were treated with coumarin-6-labeled TC-CS-SP NPs (108 μM). For a negative control, cells incubated with complete culture medium from each cell line were used. After incubation for 4 h at 37 °C, the treatment and media were removed, and the cells were washed twice with 0.5 mL PBS then harvested using trypsin. Cumulative dye release from coumarin-6-loaded TC-CS-SP NPs was analyzed under excitation at 450 nm and emission at 505 nm by flow cytometer (FACS Canto II, BD, USA).

2.2.6.4 Confocal laser microscopy. MCF7, MDA-MB-231, and HDF (1×10^5 cells per well) were seeded into a six-well plate containing glass coverslips and incubated for 24 h at 37 °C. The cells were then treated with coumarin-6-labeled TC-CS-SP NPs (108 μM) and further incubated for 4 h at 37 °C. For a negative control, cells incubated with complete culture medium from each cell line were investigated. After specified incubation time, the cells were washed with 0.5 mL of PBS, and then incubated with 0.5 mL of 4% formaldehyde at room temperature for 15 min in the dark. After that, the cells were washed again with PBS, then the PBS was removed and 300 μL of DAPI diluted in PBS (1 : 1500) was added and incubated in the dark for 5 min. Finally, the cells were washed once with 0.5 mL of PBS, and the coverslips were placed face down on a glass slide with 10 μL of Fluorescence Mounting Medium (Dako Omnis), then left to dry overnight in the dark. Samples were inspected by Zeiss LSM780 confocal microscope system (Carl Zeiss AG, Germany).[72]

3 Results and discussion

3.1 Rationale for selecting CS-SP NPs

The preparation technique was employed to synthesize intelligent CS-SP NPs. SP exhibits a low critical micelle concentration (CMC), ensuring the stability of the nano-system even upon dilution within the systemic circulation *in vivo*. Additionally, it

exhibits a lower critical solution temperature (LCST) of approximately 40 °C, which governs hydrophilic-to-hydrophobic phase transitions, directly influencing the temperature-triggered responsiveness of this intelligent nanoparticle system[73] Furthermore, CS was chosen for its compatibility and safe characteristics when incorporated into grafted nanoparticles and copolymers, displaying pH-responsive behavior.[74] The Soluplus quantity of the cross-linker, glutaraldehyde (GA), was completely eliminated through the dialysis process.

In the context of cancer treatment, the size of the nanoparticle formulation plays a pivotal role. Consequently, various molar ratios of CS-SP NPs were synthesized (100 : 1, 10 : 1, 2 : 1, 1 : 1, 1 : 2) to optimize their properties. The optimized formulation was selected based on factors such as particle size and its responsiveness to changes in temperature and pH. This optimized formulation was then used for loading the therapeutic drug (TC), which was subsequently employed in the subsequent experiments within this research study.

3.2 Physical characterization by DLS

Physiochemical properties such as hydrodynamic diameter, zeta potential, and PdI were analyzed on SP, SP : GA, CS, CS : GA, different GA crosslinked CS-SP NPs, and TC-loaded CS-SP NPs in the optimized formula. The measurements were presented in Table 1. The average particle sizes of CS and CS : GA were obtained as 593.83 ± 28.21 nm and 365.61 ± 26.33 nm, respectively. The smaller particle size of CS : GA compared to CS could indicate the crosslinking of CS with GA. Moreover, the smaller average particle size of SP : GA, which was 69.34 ± 1.41 nm, than that of SP, which was 77.23 ± 1.19 nm, can be speculated to be a crosslinking between SP and GA. Other speculation that approved the hypothesis of copolymerization of CS and SP in grafted CS-SP NPs was the average particle size and PdI of CS and SP, which showed that SP had a small particle size 77.23 ± 1.19 nm and a PdI of 0.07 ± 0.04 mV, whereas CS had a large particle size of 593.83 ± 28.21 nm and a large PdI of 0.75 ± 0.11 mV. It is suggested that the fabrication of CS-SP NPs showed a significant influence on particle size and PdI compared to pure CS or SP.

By studying the average particle size of different molar ratios of CS-SP NPs (100 : 1, 10 : 1, 2 : 1, 1 : 1, and 1 : 2), which were observed as 128.09 ± 3.61 nm, 93.09 ± 1.88 nm, 201.87 ± 4.86 nm, 86.92 ± 1.05 nm, and 101.15 ± 2.01 nm, respectively, the optimum CS-SP NPs were those with a molar ratio of 1 : 1, confirmed by trend analysis using DLS (Fig. 2). The CS-SP molar ratio that has the lowest particle size at room temperature and exhibited particle size transition at temperature near to the average temperature of breast tumor *i.e.* 37.17 to 38.44 °C[75,76] was the ratio 1 : 1. Thus, it was selected as the optimized molar ratio of CS-SP. The optimized NPs were loaded with TC and tested for the other experiments through the study.

The average particle size of the optimized molar ratio (1 : 1) of CS-SP NPs was 86.92 ± 1.05, compared to 94.17 ± 4.01 of TC-CS-SP NPs; the slight increase in particle size can be attributed to the encapsulation of the loaded TC molecules into NPs.[77] NPs

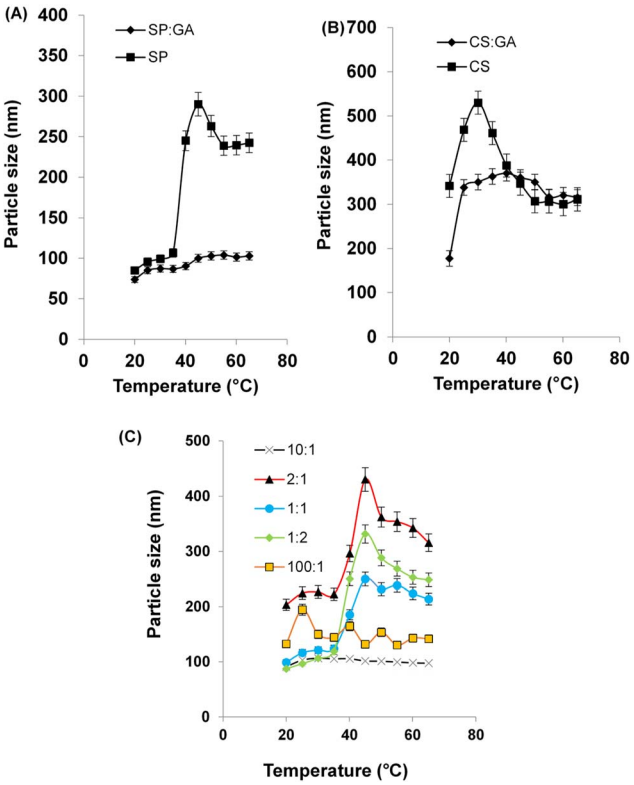

Fig. 2 Particle size *vs.* temperature curves measured by DLS for (A) SP and SP : GA, (B) CS and CS : GA, (C) five different molar ratios of CS-SP (100 : 1), (10 : 1), (2 : 1), (1 : 1), and (1 : 2) NPs.

between 10 and 100 nm in size can accomplish both intents of being small enough to avoid occlusion and clot formation when passing through the finest capillaries and large enough to bypass the rapid clearance through glomerular filtration in the kidneys.[46]

Concerning the zeta potential values, summarized in Table 1, in almost all CS-SP NPs, the zeta potential was close to neutral, with a slight increase in charge when increasing the percent of CS in NPs and a slight decrease in charge when the percent of SP was higher in NPs. As zeta potentials of 100 : 1 and 1 : 2 CS-SP NPs, were observed as 12.8 ± 4.6 and −2.5 ± 3.3, respectively. The neutrality in zeta potential can lessen the unfavorable clearance of NPs by mononuclear phagocyte system, enhance blood compatibility, henceforth, anticancer drug can be passively targeted to tumors with greater efficiency.[78]

The PdI values, also provided in Table 1, showed that all CS-SP NPs except those with a 100 : 1 molar ratio have a PdI less than 0.3. In general, PdI below 0.3 implies homogeneity of size distribution in polydispersed phase nano-formulations.[79]

3.3 Effect of temperature and pH on particle size

Concerning dual stimuli-responsive NPs, DLS verified its beneficial input in appointing temperature and pH induced physiochemical changes in NPs.[80] The different particle size responses to temperature changes from 20 to 65 °C were

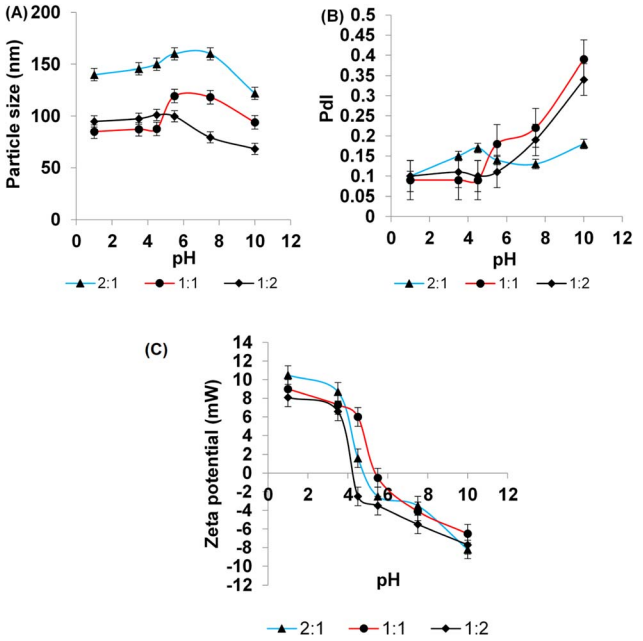

Fig. 3 The effect of pH changes on (A) particle size, (B) polydispersity index (PdI), (C) zeta potential on three different molar ratios of CS-SP NPs: (2 : 1), (1 : 1), and (1 : 2).

measured by trend analysis using DLS. The measurements were recorded as shown in Fig. 2. The LCST was examined from DLS perspective. The interpretation was corroborated with the observed phenomena reported elsewhere.[81] When temperatures were brought closer to the LCST point, the particle size increased due to the emergence of hydrophobic interactions. When the temperature exceeds the LCST, however, a reduction in size was observed. This finding might be due to a change in polymer conformation, explained by polymer chain shrinkage from loose coils to dehydrated and condensed globules.[81]

By studying Fig. 2A, SP approved its temperature-responsive behavior with a LCST in at 40 °C, as there was a noticeable particle size change from 106.6 nm to 245.1 nm. The observed phenomenon was hindered by the addition of GA to SP, which kept the particle size almost fixed upon changing temperature, confirming that SP cross-linked with GA. In Fig. 2B, it was shown that CS compared with CS cross-linked with GA had smaller particle sizes, with some effect of temperature on particle size. The copolymerization of CS and SP by the aid of GA, ascribed to neglecting the hindered effect of GA on SP thermoresponsive behavior, and the influence of temperature induced phase transition was investigated for different molar ratios of CS-SP NPs, as noticed in Fig. 2C, with the molar ratios of 100 : 1 and 10 : 1, thermoresponsive behavior was prohibited, while with 2 : 1, 1 : 1, and 1 : 2 molar ratios, phase transitions were observed at around 40 °C.

Upon varied pH values, the pH sensitivity of NPs can be studied by determining the change in hydrodynamic diameter and the zeta potential of the NPs.[82] To estimate the effect of pH for formulations that had shown temperature phase transition previously, measurements were carried out and results as shown in Fig. 3. The change in pH for different CS-SP NPs was adjusted within the pH range of 1.0–12.0 by the addition of either 0.1 M HCL or 0.1 M NaOH. Fig. 3A confirmed that there was no significant change in particle size in CS-SP NPs when the pH range was from 1.0 to 4.5, with a significant increase in size from 87.5 ± 1.6 to 119.4 ± 3.3 in 1 : 1 molar ratio of CS-SP NPs when pH changed from 4.5 to 5.5. This result pointedly supports the proposed hypothesis of pH-responsive behavior of these NPs when reaching pH that represents a slightly acidic microenvironment of cancerous cell.

CS-SP-NPs with a molar ratio of 2 : 1 had a bigger particle size than 1 : 1 and 1 : 2 molar ratios. In addition, in CS-SP-NPs with a molar ratio of 1 : 2, the effect of pH on particle size had not appeared to be as great, as CS appeared to have a lesser contribution in comparison with a 1 : 1 molar ratio. The optimized formula had a molar ratio of 1 : 1, supported by its pH and temperature responsive behavior, which appeared as a change in particle size upon a change in temperature or pH. PdI values are shown in Fig. 3B. The values indicated the presence of an almost monodisperse particle size distribution with a PdI lower than 0.3 through pH changes from 1.0 to 7.5. A polydispersity that appears in alkaline pH, might be attributed to different precipitation of NPs in alkaline media. In Fig. 3C, the zeta potential for 1 : 2, 1 : 1, and 2 : 1 CS-SP-NPs molar ratios had a positive value when shifted toward acidic pH and a negative value when shifted toward alkaline pH, supported by protonation–deprotonation of CS at different pH values.[83]

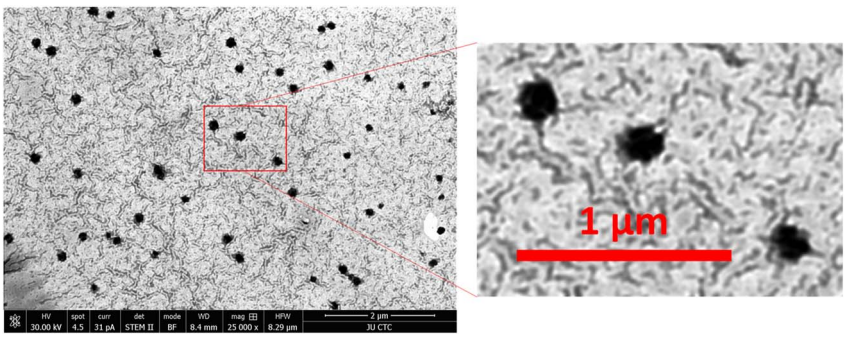

Fig. 4 STEM images of optimal CS-SP NPs, where CS and SP were prepared at optimal molar ratios (1 : 1). The scale bar is 1 and 2 µm.

3.4 Determination of EE and DL

The measured percentages of EE and DL, in the optimal formula CS-SP of molar ratio 1 : 1, were recorded as 96.66 ± 1.5% and 17.50 ± 0.21% w/w, respectively. By considering the hydrophobic characteristic of TC and the preferable loading of TC into CS-SP NPs, as indicated by the high EE, these NPs offer a promising approach as a carrier for one or more hydrophobic drugs, particularly anticancer drugs.

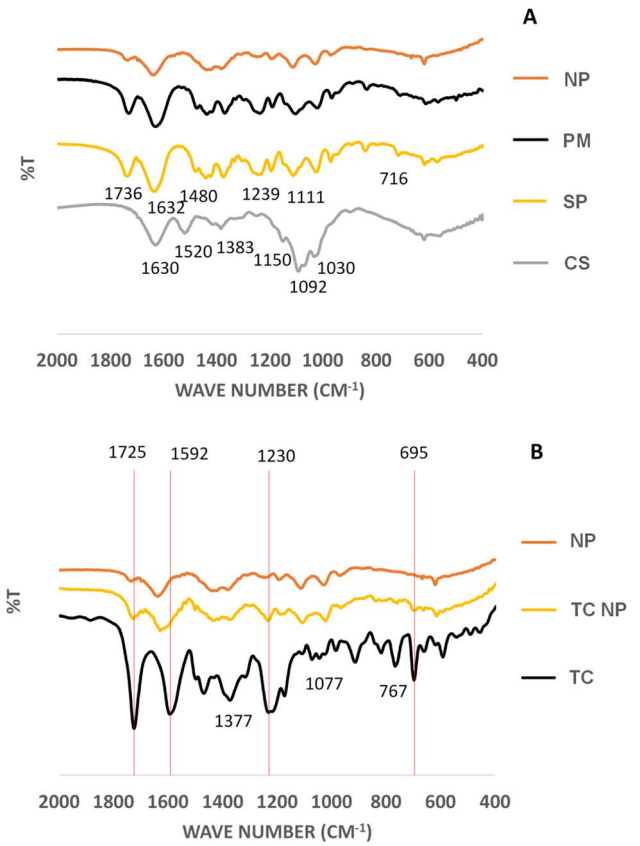

Fig. 5 FTIR spectrum of (A) chitosan (CS), Soluplus (SP), CS-SP physical mixture (PM) and CS-SP prepared nanoparticles prepared by crosslinking with glutaraldehyde (NP), where CS and SP were prepared at optimal molar ratios (1 : 1), (B) NPs, tamoxifen citrate (TC) and tamoxifen citrate loaded CS-SP NP (TC NP).

3.5 Morphology of nanoparticles

The morphological characterization of optimal TC-CS-SP NPs was examined by STEM with negative staining. The image indicates spherical shaped NPs with a smooth surface and a homogenous size distribution, Fig. 4. In general, the morphology of block copolymer micelle is spherical.[84]

3.6 Fourier transform infrared (FTIR) spectroscopy

FTIR analysis was carried out for CS, SP, TC, CS-SP physical mixture, CS-SP NPs, TC-CS-SP physical mixture, and TC-CS-SP NPs, as shown in Fig. 5, in order to emphasize the copolymerization of CS and SP.

The IR spectrum showed distinct peaks of CS functional groups, which were 1630 cm^{-1} and 1520 cm^{-1} for NH_2 stretching group, 1383 cm^{-1} CH stretching group,1150 cm^{-1} for β(1–4) glycosidic bridge, 1092 cm^{-1} and 1030 cm^{-1} for –C–O–C– bridge.[85–87] The characteristics peaks of SP were 1736 cm^{-1} and 1632 cm^{-1} for carbonyl stretching group in ester and tertiary amide, respectively, 1480 cm^{-1} for C–O–C stretching group, 1239 cm^{-1} and 1111 cm^{-1} for C–O stretching group in ester and 716 cm^{-1} for CH bending group.[88] The featured peaks of TC were revealed as 1725 cm^{-1} for carbonyl stretching group, 1592 cm^{-1} for amine N–H bending group, 1377 cm^{-1} for methyl group, 1077 cm^{-1} for C–N stretching group; 1230 cm^{-1} refer to C–O stretching of alkyl aryl ether. Peaks were also observed at 767 cm^{-1} and 695 cm^{-1}.[89]

Upon mixing CS with SP in the physical mixture (PM) the FTIR did not show the peaks of CS polymer may be due to the similarity and dilution effect due to molecular weight differences as shown in (Fig. 5A). The decrease or even absence of the peaks at 1736 cm^{-1} and 1239 cm^{-1} for C═O carbonyl stretching group in ester and C–O–C backbone of SP respectively for the CS-SP NPs compared to physical mixture could indicate the cross-linking of NP by GA was achieved.

Further construing the FTIR spectra of TC and TC-CS-SP NPs (Fig. 5B), it was noticed that the functional groups of TC were present with almost no significant changes in the TC loaded CS-SP NP. This could indicate that the drug was physically encapsulated within CS-SP NPs. The peak of TC at 1592 cm^{-1} was shifted in the CS-SP NP system. The shifting of this peak might

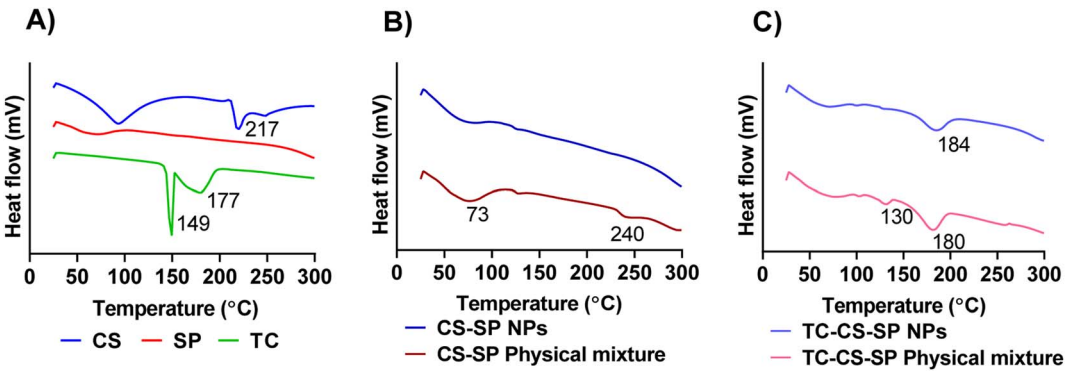

Fig. 6 DSC spectra of (A) CS, SP and TC, (B) CS-SP NPs and CS-SP physical mixture, (C) TC-CS-SP NPs and TC-CS-SP physical mixture.

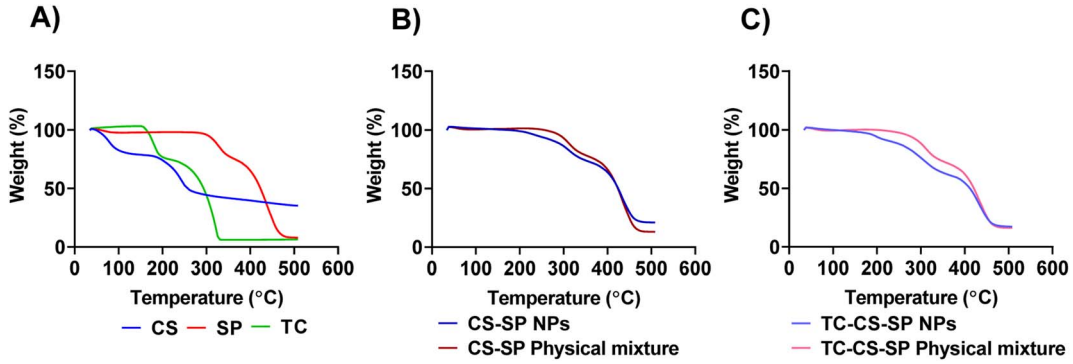

Fig. 7 TGA curve of (A) CS, SP and TC, (B) CS-SP NPs and CS-SP physical mixture, (C) TC-CS-SP NPs and TC-CS-SP physical mixture prepared at optimal CS to SP molar ratios (1 : 1).

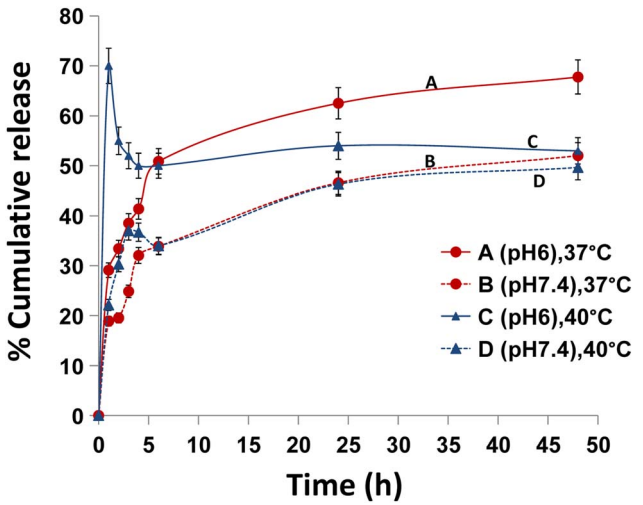

Fig. 8 *In vitro* release study of TC from TC-CS-SP NPs prepared at optimal CS to SP molar ratios (1 : 1) at (A) 37 °C and pH 6, (B) 37 °C and pH 7.4, (C) 40 °C and pH 6, (D) 40 °C and pH 7.4.

have taken place due to the weak physical interaction of weak H-bonding with the CS-SP NP system.

3.7 Differential scanning calorimetry (DSC) analysis

The thermograms reported in Fig. 6A showed that the glass transition temperature of SP is measured at around 70 °C, the melting point peak of TC is observed at 149 °C, followed by chemical degradation of the drug at 177 °C, and CS is represented by the a broad endothermic peak from 50 to 110 °C that can be correlated to the loss of moisture, followed by CS degradation at 217 °C.[90,91]

Based on Fig. 6B, the disappearance of the thermal event that can be attributed to the degradation of CS, obtained at 240 °C in CS-SP NPs, compared to the peak presented in the CS-SP physical mixture, indicated a chemical cross-linking of CS and SP in NPs. In CS-SP NPs, the cross-linked CS was protected from chemical degradation, which was not the case in CS-SP physical mixture. These results confirmed the cross-linking and copolymerization of the two polymers in CS-SP NPs. In addition, with DSC thermogram of TC-CS-SP NPs that is shown in Fig. 6C. A new melting point of TC at 130 °C was observed in the physical mixture. This change in the melting point could be due to the interaction between the components of the mixture. The absence of the TC melting peak at 130 °C suggests that TC was successfully encapsulated into CS-SP NPs.

3.8 Thermogravimetric analysis (TGA)

TGA curves for CS, SP, CS-SP physical mixture, CS-SP NPs, TC-CS-SP physical mixture, and TC-CS-SP NPs are shown in Fig. 7A. There was an initial weight loss in CS curve from 25 °C to 110 °C due to evaporation of water; the second weight loss was owed to polymer decomposition from 200 °C to 300 °C.[92]

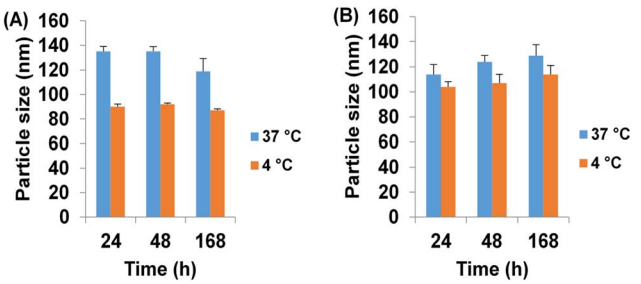

Fig. 9 Particle size of stability analysis for TC-CS-SP NPs prepared at optimal CS to SP molar ratios (1 : 1) incubated at 37 °C and 4 °C, at: (A) phosphate buffer pH 6, (B) phosphate buffer pH 7.4. Error bar indicate SD ($n = 3$).

Table 2 Zeta potential for TC-CS-SP NPs prepared at optimal CS to SP molar ratios (1 : 1) incubated at different phosphate bufsfer (pH 6, pH 7.4) at different temperature (mean ± SD, $n = 3$)

Zeta potential (mV)				
Temperature	37 °C		4 °C	
Time (h)	pH 7.4	pH 6	pH 7.4	pH 6
24	−1.6 ± 0.6	0.4 ± 0.3	−1.6 ± 0.4	0.8 ± 0.5
48	−2.3 ± 0.1	−0.1 ± 0.5	−2.7 ± 0.9	0.7 ± 0.4
168	−3.8 ± 0.4	1.5 ± 0.6	−0.6 ± 0.4	0.8 ± 0.4

Meanwhile, in SP curve, as the temperature increased, an initial weight loss was founded due to moisture evaporation over around 100 °C; an additional weight loss was monitored due to degradation of the polymer when the temperature increased to 300 °C, which was recorded as thermal degradation temperature of SP.[93] TC has begun to degrade at 170 °C with a complete degradation over 300 °C.[94] No significant difference in thermal behavior was noticed by comparing the TGA curves of CS-SP NPs and CS-SP physical mixture provided in Fig. 7B.

The thermal behavior of TC-CS-SP NPs was similar to that of CS-SP NPs (Fig. 7C), suggesting that the existence of TC in drug payload NPs did not significantly alter the physicochemical stability of the NPs.[67,94]

3.9 *In vitro* drug release

Studies of drug release can serve as concept verification for the stimuli-responsiveness of nanoparticles. As selective delivery is accomplished by stimuli that alter micelle structure and trigger drug release like change in pH, specific enzymes, availability of reducing agents, light, ultrasounds, and temperature.[95] If the amount of drug released when reaching the tumor is not much more than that released in the circulation, herein the extent of response of a stimuli sensitive nanocarrier would not be sufficient to enhance the therapeutic efficacy of the drug, and the response achieved from a responsive nanocarrier may be as effective as that achieved by a nonresponsive system.[96]

The most typical method used to characterize drug release from micelles is dialysis.[97] The drug release behavior of TC-CS-SP NPs was investigated in simulated physiological conditions: Tris-HCL (pH 7.4) and simulated medium represent the tumor microenvironment; Tris-HCL (pH 6) which used to evaluate the pH sensitivity of TC-CS-SP NPs. And different temperatures (37 ± 2 or 40 ± 2 °C) were applied to evaluate the thermoresponsive behavior of TC-CS-SP NPs. The *in vitro* drug release was conducted for 48 h, and the percent drug release was established by monitoring the concentration of TC released at prescheduled time points, based on the calibration curve of TC. Fig. 8, the TC release rate and amount at 40 °C in pH 6 medium were more dramatic than those at 37 °C in the same release medium pH, with 70% and 29% of drug release within 1 h, respectively, displaying a clear evident of temperature triggered release. The phase transition behavior of CS-SP NPs at their LCST is responsible for the burst release of the entrapped drug at 40 °C. This result in drug diffusing out faster might be due to the less rigidity of the copolymer micelles near LCST. However, after the burst drug release in pH 6 at 40 °C, TC started to precipitate in the dissolution media, lowering the quantified TC by HPLC for

Table 3 PdI for TC-CS-SP NPs prepared at optimal CS to SP molar ratios (1 : 1) incubated at different phosphate buffer (pH 6, pH 7.4) at different temperature (mean ± SD, $n = 3$)

PdI				
Temperature	37 °C		4 °C	
Time (h)	pH 7.4	pH 6	pH 7.4	pH 6
24	0.3	0.3	0.3	0.2
48	0.3	0.3	0.3	0.2
168	0.4	0.3	0.3	0.2

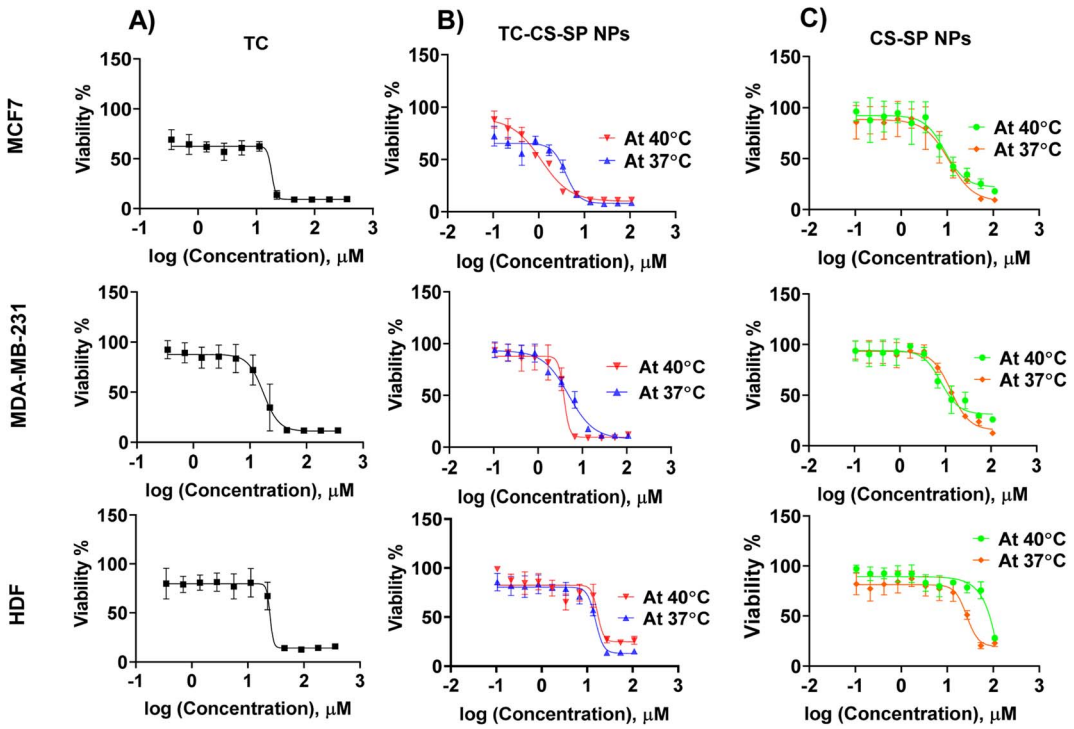

Fig. 10 Cytotoxic effect as a concentration response curve of (A) free TC, (B) TC-CS-SP NPs prepared at optimal CS to SP molar ratios (1 : 1) at 37 °C and 40 °C, (C) CS-SP NPs at 37 °C and 40 °C incubated with MCF7, MDA-MB-231 and HDF cell lines, using MTT assay.

the next specified time intervals, as it was difficult to grant that *in vitro* conditions represent *in vivo* conditions.

In addition, TC release pattern at physiological temperature (37 °C) was considerably faster from TC-CS-SP NPs in acidic medium (pH 6) than in pH 7.4, with 50% and 33% of the entrapped release after 6 h, respectively. This indicated a pH-dependent release profile for TC-loaded CS-SP NPs.

In comparison, at physiological pH (7.4), controlled release was observed when TC-CS-SP NPs were incubated at 37 °C or 40 °C, with about 50% drug release over 48 h in both cases, indicating no significant difference in release pattern. It might be that the temperature-triggered release is significantly accelerated by changing pH from 7.4 to 6.0.[96]

By considering the challenging drawbacks of cancer treatment, smart nanoparticle systems are designed to selectively deliver anticancer drugs to tumor tissues with the help of the tumor microenvironment, which is distinguished by its slightly acidic pH and slightly elevated temperature compared to physiological pH and temperature. The pH and temperature-triggered release behavior of TC from these fabricated NPs could eliminate its massive side effects over the course of a long-term treatment and improve patient compliance.

3.10 Determination of physical stability

The physical stability of TC-CS-SP NPs were assessed in different conditions with respect to temperature and pH, as the test was conducted in different phosphate buffer (pH 6 or 7.4), incubated at different temperatures (37 °C or 4 °C). Based on particle size, zeta potential, and PdI, the judgment was performed. As displayed

Table 4 IC_{50} values of MTT assay after incubating the treatments with the cells

IC_{50} (μM)					
Treatment	TC	TC-CS-SP NPs[a] at 37 °C	TC-CS-SP NPs at 40 °C	CS-SP NPs[a] at 37 °C	CS-SP NPs[a] at 40 °C
MCF7	18.31 ± 2.44	3.89 ± 0.33	1.12 ± 0.42	10.97 ± 3.37	8.94 ± 3.63
MDA-MB-231	17.24 ± 2.86	3.84 ± 0.47	4.84 ± 0.67	13.14 ± 1.29	8.04 ± 3.80
HDF	24.89 ± 2.26	15.07 ± 1.20	16.84 ± 2.59	26.29 ± 1.67	>100

[a] NPs were prepared at optimal CS to SP molar ratios (1 : 1).

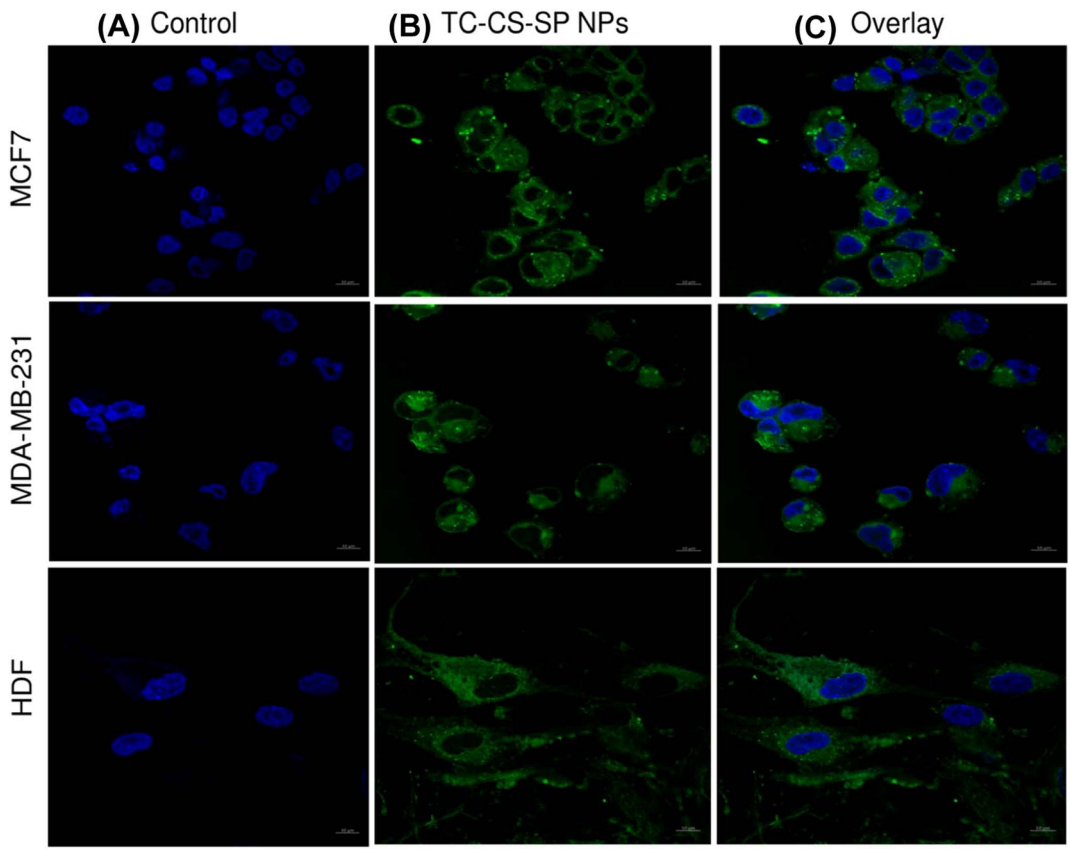

Fig. 11 Confocal laser scanning microscopy images of MCF7, MDA-MB-231 and HDF. (A) Control cell nuclei (blue) stained by DAPI, (B) TC-CS-SP NPs inside the cytoplasm (green), (C) overlay shows TC-CS-SP NPs accumulation prepared at optimal CS to SP molar ratios (1 : 1).

in Fig. 9, the measurements of particle size revealed that particle size is not affected by time; there is no aging in all incubation media, irrespective of the change in temperature. Zeta potential values, as given in Table 2, indicated that NPs had a neutral and stable charge throughout the study. In addition, referring to Table 3, a homogenous particle size distribution was observed with PdI values equal or less than 0.3. Particle size of NPs incubated at 37 °C was comparatively larger than that of NPs incubated at 4 °C in slightly acidic conditions. This observation confirmed the results obtained from the previous analysis of the behavior of CS-SP NPs with respect to changes in pH and temperature.[98]

3.11 Cell viability assay

In MTT assay, non-cancerous HDF and breast cancer cell lines MCF7 and MDA-MB-231 were treated with free TC, blank CS-SP NPs, and TC-CS-SP NPs for 72 h at various concentrations from 0.1 to 108 μM. Results of cell viability assay, displayed in Fig. 10, were presented as a concentration response curve, which revealed a concentration-dependent sensitivity of the drug against all tested cell lines. The judgments were based on IC_{50} values, which were provided in Table 4, and the viable cells were calculated for each concentration by considering the 100% viable cells in control samples as a reference. The IC_{50} values of TC-CS-SP NPs were 3.89 ± 0.33 μM and 3.84 ± 0.47 μM for MCF7 and MDA-MB-231 cell lines, respectively, whereas the IC_{50} values exerted when treated with free TC were 18.31 ± 2.44 μM for MCF7 cells and 17.24 ± 2.86 μM for MDA-MB-231 cells. The observed results leading by a remarkable reduction in IC_{50} values and enhanced cytotoxicity up to 4.5-fold in both cell lines, indicating excellent drug loaded nanoparticle uptake, enhanced permeation, and increased intracellular drug accumulation, confirmed by a lower concentration of TC needed to induce the anti-tumor effect in TC-CS-SP NPs.

In a further experiment to investigate the thermoresponsive behavior of CS-SP NPs supported by their LCST at 40 °C, which was previously assessed by DLS, MTT assay was also conducted at 40 °C by incubating the treated cell lines at 40 °C for 5 min every 24 h. By comparing the IC_{50} values reported at 37 °C and 40 °C, it was found that the cytotoxicity was significantly increased by 3.5 times by the use of TC-CS-SP NPs when incubated at 40 °C compared to 37 °C, with IC_{50} values of 1.12 ± 0.42

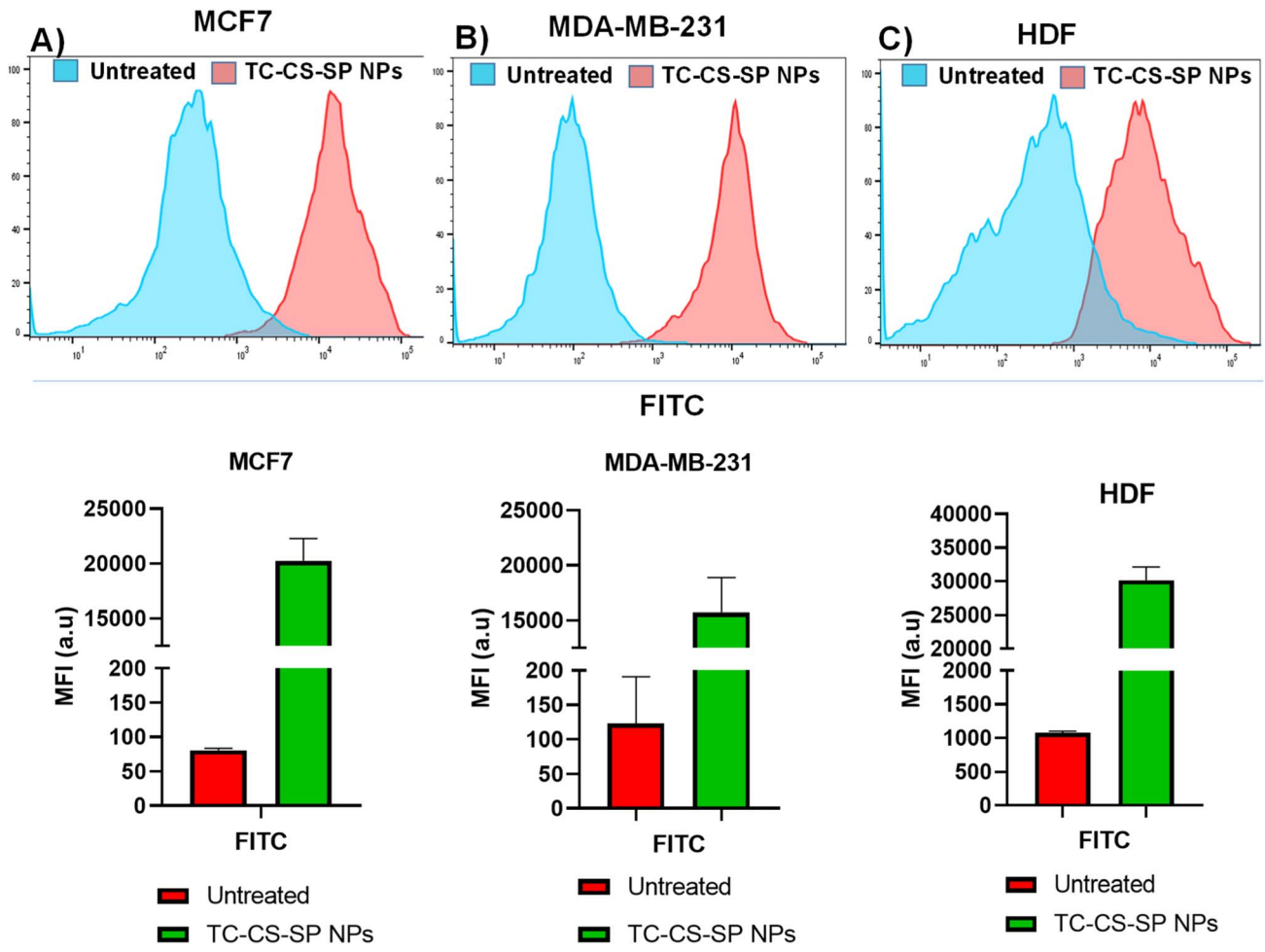

Fig. 12 Flow cytometry analysis for cellular uptake of labeled TC-CS-SP NPs prepared at optimal CS to SP molar ratios (1 : 1) in cultured cell lines; (A) MCF7, (B) MDA-MB-231, (C) HDF. Upper part of A, B, C; show flow cytometry histogram of treated cells with TC-CS-SP NPs compared to untreated cells. Lower part of A, B, C; show mean fluorescence intensity measurements (MFI) of TC-CS-SP NPs compared to untreated cells.

μM and 3.89 ± 0.33 μM, respectively, in MCF7 cell line. The observable decline in IC_{50} value and the improved efficacy of TC-CS-SP NPs at 40 °C mainly contributed to accelerating the release of TC at the LCST of NPs, which was previously approved by the *in vitro* drug release study.

In MDA-MB-231 cell line, there was no significant effect of temperature on cytotoxicity, as there was no significant difference in the IC_{50} value at 37 °C, which was 3.84 ± 0.47 μM, and at 40 °C, which was 4.84 ± 0.67 μM. The possible explanation that underlies the negligible difference in cytotoxicity is that MDA-MB-231 cells are composed of ER-cancerous cells, while TC mainly acts on ER+ cancer cells.

The IC_{50} value of HDF cell line treated with blank CS-SP NPs at 37 °C or 40 °C emphasized the biocompatibility of NPs that showed a relatively higher IC_{50} value to induce cytotoxicity, indicating the non-toxicity of CS-SP NPs.

3.12 Cellular uptake study

Cell uptake and internalization of TC-CS-SP NPs were examined qualitatively by confocal microscopy and quantitatively by flow cytometry analysis. Labeled fluorescent coumarin-6-loaded TC-CS-SP NPs were prepared to signify the cellular uptake of TC-CS-SP NPs by MCF7, MDA-MB-231, and HDF cell lines, as TC cannot be visualized under CLSM. The nucleus of each cell line was stained with DAPI. As demonstrated in Fig. 11, DAPI stain was responsible for the blue fluorescence of nuclei, while the green fluorescence emanated from coumarin-6-labeled TC-CS-SP NPs. The endocytosis and preferential localization of TC-CS-SP NPs in the cytoplasm and perinuclear zone were observed in all tested cell lines (Fig. 11C).

Furthermore, the high uptake of TC is evidently tracked and noticed within 4 h of incubation with cells by flow cytometry. A mean florescent intensity, as given in Fig. 12, showed a remarkable cellular uptake of labeled TC-CS-SP NPs by MCF7 cells, with a 250-fold increase in uptake between treated and untreated cells, and with a 128-fold increase in uptake between treated and untreated cells by MDA-MB-231 cells. A lower cellular uptake was shown in HDF cells with a 28-fold increase between treated and untreated cells, which correlated with the biocompatibility and safety profile of these NPs emphasized with the MTT assay. The superior uptake of NPs by MCF7 cells compared to MDA-MB-231cells can be ascribed to the estrogen receptors expressed in MCF7 cells, where TC mainly acts as an anti-tumor agent and shows its inhibitory effect.

4 Conclusion

Our findings suggest that CS-SP NPs has a great potential to consider as a safe and robust smart nanocarrier in delivering TC selectively to tumor cells based on dual stimuli-triggered response as the attempts made to copolymerization of pH and thermo-sensitive polymers achieve both goals of this study. CS SP NP were characterized to have high entrapment efficiency, high cellular uptake and cytotoxicity against cancerous cells influenced by the distinct characteristics of tumor microenvironment. The loading of TC in CS-SP NPs resulted in significant enhancement of solubility and subsequently improving the cellular uptake of the hydrophobic BCS class II anticancer drug (tamoxifen citrate). The *in vitro* release studies indicated that CS SP NPs can be used to deliver TC safely with an adequate loaded amount to the targeted cancerous area.

Conflicts of interest

Authors have no conflict of interest to declare.

Acknowledgements

The authors acknowledge the research fund provided by the Deanship of Research of the University of Petra.

References

1 A. Moin, S. U. D. Wani, R. A. Osmani, A. S. Abu Lila, E.-S. Khafagy, H. H. Arab, H. V. Gangadharappa and A. N. Allam, *Drug delivery*, 2021, **28**, 1626–1636.
2 N. Harbeck, F. Penault-Llorca, J. Cortes, M. Gnant, N. Houssami, P. Poortmans, K. Ruddy, J. Tsang and F. Cardoso, *Nat. Rev. Dis. Primers*, 2019, **5**, 66.
3 C. M. Day, S. M. Hickey, Y. Song, S. E. Plush and S. Garg, *Molecules*, 2020, **25**, 1182.
4 M. C. Farrar and T. F. Jacobs, in *StatPearls [Internet]*, StatPearls Publishing, 2022.
5 N. SreeHarsha, J. G. Hiremath, S. Chilukuri, R. K. Aitha, B. E. Al-Dhubiab, K. N. Venugopala, A. M. Alzahrani and G. Meravanige, *BioMed Res. Int.*, 2019, **2019**, 2161348.
6 A. Bose, D. Roy Burman, B. Sikdar and P. Patra, *IET Nanobiotechnol.*, 2021, **15**, 19–27.
7 B. Tian, S. Liu, S. Wu, W. Lu, D. Wang, L. Jin, B. Hu, K. Li, Z. Wang and Z. Quan, *Colloids Surf., B*, 2017, **154**, 287–296.
8 C. Pucci, C. Martinelli and G. Ciofani, *Ecancermedicalscience*, 2019, **13**, 961.
9 H. Havel, G. Finch, P. Strode, M. Wolfgang, S. Zale, I. Bobe, H. Youssoufian, M. Peterson and M. Liu, *AAPS J.*, 2016, **18**, 1373–1378.
10 S. Ghosh, K. Ghosal, S. A. Mohammad and K. Sarkar, *Chem. Eng. J.*, 2019, **373**, 468–484.
11 H. Maeda, *Adv. Drug Delivery Rev.*, 2015, **91**, 3–6.
12 M. Al-Remawi, N. Jaber, A. Elsayed, D. Alsafadi and K. A. Salah, *Carbohydr. Polym.*, 2022, **291**, 119579.
13 J. Shi, P. W. Kantoff, R. Wooster and O. C. Farokhzad, *Nat. Rev. Cancer*, 2017, **17**, 20–37.
14 M. Srinivasan, M. Rajabi and S. A. Mousa, *Nanomaterials*, 2015, **5**, 1690–1703.
15 U. Prabhakar, H. Maeda, R. K. Jain, E. M. Sevick-Muraca, W. Zamboni, O. C. Farokhzad, S. T. Barry, A. Gabizon, P. Grodzinski and D. C. Blakey, *Cancer Res.*, 2013, **73**, 2412–2417.
16 M. T. Manzari, Y. Shamay, H. Kiguchi, N. Rosen, M. Scaltriti and D. A. Heller, *Nat. Rev. Mater.*, 2021, **6**, 351–370.
17 Y. Dai, C. Xu, X. Sun and X. Chen, *Chem. Soc. Rev.*, 2017, **46**, 3830–3852.

18 B. Ghosh and S. Biswas, *J. Controlled Release*, 2021, **332**, 127–147.
19 N. Jaber, M. Al-Remawi, L. A. Qatouseh, M. Ahmad and K. Aiedeh, *J. Drug Delivery Sci. Technol.*, 2020, **58**, 101761.
20 G. V. Bonde, S. K. Yadav, S. Chauhan, P. Mittal, G. Ajmal, S. Thokala and B. Mishra, *Expert Opin. Drug Delivery*, 2018, **15**, 495–507.
21 L. Zhu, F. Perche, T. Wang and V. P. Torchilin, *Biomaterials*, 2014, **35**, 4213–4222.
22 C. Altinkok, G. Acik, H. R. F. Karabulut, M. Ciftci, M. A. Tasdelen and A. Dag, *Polym. Adv. Technol.*, 2021, **32**, 4860–4868.
23 S. M. Tawfik, S. Azizov, M. R. Elmasry, M. Sharipov and Y.-I. Lee, *Nanomaterials*, 2020, **11**, 70.
24 A. Alsuraifi, A. Curtis, D. A. Lamprou and C. Hoskins, *Pharmaceutics*, 2018, **10**, 136.
25 Y. Zhang, J. Yu, H. N. Bomba, Y. Zhu and Z. Gu, *Chem. Rev.*, 2016, **116**, 12536–12563.
26 E. González and M. W. Frey, *Polymer*, 2017, **108**, 154–162.
27 D. Chang, Y. Ma, X. Xu, J. Xie and S. Ju, *Front. bioeng. biotechnol.*, 2021, **9**, 707319.
28 S. Y. Lee, S. Nam, Y. Choi, M. Kim, J. S. Koo, B.-J. Chae, W.-S. Kang and H.-J. Cho, *Appl. Sci.*, 2017, **7**, 902.
29 A. Abu-Rumman, R. Abu-Huwaij and R. Hamed, *J. Adhes.*, 2022, **98**, 915–933.
30 M. Pozzoli, D. Traini, P. M. Young, M. B. Sukkar and F. Sonvico, *Drug Dev. Ind. Pharm.*, 2017, **43**(9), 1510–1518.
31 C. Sofroniou, M. Baglioni, M. Mamusa, C. Resta, J. Doutch, J. Smets and P. Baglioni, *ACS Appl. Mater. Interfaces*, 2022, **14**, 14791–14804.
32 M. A. Kennedy, Y. Zhang and S. R. Bhatia, *Nanotechnology*, 2023, **34**, 125602.
33 A. Salawi and S. Nazzal, *Int. J. Pharm.*, 2018, **546**, 255–262.
34 Y. Zhong, G. Jing, B. Tian, H. Huang, Y. Zhang, J. Gou, X. Tang, H. He and Y. Wang, *Asian J. Pharm. Sci.*, 2016, **11**, 255–264.
35 G. M. Metilda and J. P. Kumari, *Int. J. Pharm. Sci. Res.*, 2016, **7**, 681.
36 R. Takayama, M. Ishizawa, M. Yamada, Y. Inoue and I. Kanamoto, *ChemEngineering*, 2021, **5**, 44.
37 R. Shanmuganathan, T. N. J. I. Edison, F. LewisOscar, P. Kumar, S. Shanmugam and A. Pugazhendhi, *Int. J. Biol. Macromol.*, 2019, **130**, 727–736.
38 T. Reintjes, *Solubilizer Compendium*, 2011.
39 R. Pignatello and R. Corsaro, *Curr. Nanomed.*, 2019, **9**, 184–197.
40 R. S. Bhuptani, A. S. Jain, D. T. Makhija, A. G. Jagtap, P. A. R. Hassan and M. S. Nagarsenker, *Indian J. Pharm. Educ. Res.*, 2016, **50**, 277–286.
41 R. Pignatello, R. Corsaro, A. Bonaccorso, E. Zingale, C. Carbone and T. Musumeci, *Drug Delivery Transl. Res.*, 2022, 1–16.
42 F. Al-Akayleh, N. Jaber and M. Al-Remawi, *J. Pharm. Innovation*, 2020, 1–13.
43 S. H. Pham, Y. Choi and J. Choi, *Pharmaceutics*, 2020, **12**, 630.
44 S.-C. Liao, C.-W. Ting and W.-H. Chiang, *J. Colloid Interface Sci.*, 2020, **561**, 11–22.
45 Y. Liu, W. Wang, J. Yang, C. Zhou and J. Sun, *Asian J. Pharm. Sci.*, 2013, **8**, 159–167.
46 N. Majumder, N. G. Das and S. K. Das, *Ther. Delivery*, 2020, **11**, 613–635.
47 J. Li, C. Cai, J. Li, J. Li, J. Li, T. Sun, L. Wang, H. Wu and G. Yu, *Molecules*, 2018, **23**, 2661.
48 M. J. Masarudin, S. M. Cutts, B. J. Evison, D. R. Phillips and P. J. Pigram, *Nanotechnol., Sci. Appl.*, 2015, **8**, 67.
49 L. Tavares, E. E. E. Flores, R. C. Rodrigues, P. F. Hertz and C. P. Z. Noreña, *Food Hydrocolloids*, 2020, **106**, 105876.
50 S. Khoee, A. Saadatinia and R. Bafkary, *Ultrason. Sonochem.*, 2017, **39**, 144–152.
51 F. Al-Akayleh, N. Jaber, M. Al-Remawi, G. Al Odwan and N. Qinna, *Pharm. Dev. Technol.*, 2022, **27**, 479–489.
52 P. Gao, G. Xia, Z. Bao, C. Feng, X. Cheng, M. Kong, Y. Liu and X. Chen, *Int. J. Biol. Macromol.*, 2016, **91**, 716–723.
53 V. Piazzini, M. Vasarri, D. Degl'Innocenti, A. Guastini, E. Barletta, M. C. Salvatici and M. C. Bergonzi, *Pharmaceutics*, 2019, **11**, 655.
54 A. Baroudi, C. García-Payo and M. Khayet, *Polymers*, 2018, **10**, 117.
55 S. Zhang, P. Zhu, J. He, S. Dong, P. Li, C. Y. Zhang and T. Ma, *Adv. Healthcare Mater.*, 2020, **9**, 2000387.
56 M. Shahriari, V. P. Torchilin, S. M. Taghdisi, K. Abnous, M. Ramezani and M. Alibolandi, *Biomater. Sci.*, 2020, **8**, 5787–5803.
57 B.-l. Ye, R. Zheng, X.-j. Ruan, Z.-h. Zheng and H.-j. Cai, *Biochem. Biophys. Res. Commun.*, 2018, **495**, 414–420.
58 S. Hosseini Sadr, S. Davaran, E. Alizadeh, R. Salehi and A. Ramazani, *J. Biomater. Sci., Polym. Ed.*, 2018, **29**, 277–308.
59 R. Safdar, A. A. Omar, A. Arunagiri, I. Regupathi and M. Thanabalan, *J. Drug Delivery Sci. Technol.*, 2019, **49**, 642–659.
60 K. Öztürk-Atar, M. Kaplan and S. Çalış, *Drug Dev. Ind. Pharm.*, 2020, **46**, 1695–1704.
61 J. F. Alopaeus, E. Hagesæther and I. Tho, *Pharmaceuticals*, 2019, **12**, 15.
62 R. P. Johnson, Y. I. Jeong, J. V. John, C.-W. Chung, D. H. Kang, M. Selvaraj, H. Suh and I. Kim, *Biomacromolecules*, 2013, **14**, 1434–1443.
63 J. Hiremath, C. Rudani, R. Suthar and A. Domb, *J. Drug Delivery Sci. Technol.*, 2011, **21**, 417–422.
64 C. Chunhachaichana and T. Srichana, *J. Dispersion Sci. Technol.*, 2019, **40**, 1461–1468.
65 G. Graverini, V. Piazzini, E. Landucci, D. Pantano, P. Nardiello, F. Casamenti, D. E. Pellegrini-Giampietro, A. R. Bilia and M. C. Bergonzi, *Colloids Surf., B*, 2018, **161**, 302–313.
66 D. Gozali, I. Sopyan, H. Hairunnisa and S. S. Marvita, *Indones. J. Chem.*, 2022, **22**, 478–490.
67 E. Pérez, M. Benito, C. Teijon, R. Olmo, J. M. Teijón and M. D. Blanco, *J. Microencapsulation*, 2012, **29**, 309–322.
68 Y. Dai, D. Wu, S. Lin, X. Ma, X. Zhang and F. Xia, *J. Nanopart. Res.*, 2019, **21**, 1–10.
69 H. Wang and A. Ullah, *Polymers*, 2022, **14**, 3436.
70 L. Deng, J. Ren, J. Li, J. Leng, Y. Qu, C. Lin and D. Shi, *Nanoscale*, 2015, **7**, 9655–9663.

71 A. K. Jain, N. K. Swarnakar, C. Godugu, R. P. Singh and S. Jain, *Biomaterials*, 2011, **32**, 503–515.
72 W. Alshaer, H. Hillaireau, J. Vergnaud, S. Ismail and E. Fattal, *Bioconjugate Chem.*, 2015, **26**, 1307–1313.
73 C. Chakrabarti, S. A. Pillai, K. Kuperkar, D. Ray, V. K. Aswal and P. Bahadur, *J. Mol. Liq.*, 2022, **349**, 118158.
74 Y. Liang, X. Zhao, P. X. Ma, B. Guo, Y. Du and X. Han, *J. Colloid Interface Sci.*, 2019, **536**, 224–234.
75 T. Yahara, T. Koga, S. Yoshida, S. Nakagawa, H. Deguchi and K. Shirouzu, *Surg. Today*, 2003, **33**, 243–248.
76 Q. Zhao, J. Zhang, R. Wang and W. Cong, *IEEE eng. med. biol. mag.*, 2008, **27**, 64–66.
77 P. Ramalingam and Y. T. Ko, *Colloids Surf., B*, 2016, **139**, 52–61.
78 F. L. Campos, J. de Alcântara Lemos, C. M. R. Oda, J. de Oliveira Silva, R. S. Fernandes, S. E. M. Miranda, C. H. Cavalcante, G. D. Cassali, D. M. Townsend and E. A. Leite, *Polymers*, 2022, **14**, 4905.
79 M. Danaei, M. Dehghankhold, S. Ataei, F. Hasanzadeh Davarani, R. Javanmard, A. Dokhani, S. Khorasani and M. Mozafari, *Pharmaceutics*, 2018, **10**, 57.
80 M. Ghezzi, S. Pescina, C. Padula, P. Santi, E. Del Favero, L. Cantù and S. Nicoli, *J. Controlled Release*, 2021, **332**, 312–336.
81 M. Lemanowicz, A. Gierczycki, W. Kuźnik, R. Sancewicz and P. Imiela, *Miner. Eng.*, 2014, **69**, 170–176.
82 Y. Luo, X. Yin, X. Yin, A. Chen, L. Zhao, G. Zhang, W. Liao, X. Huang, J. Li and C. Y. Zhang, *Pharmaceutics*, 2019, **11**, 176.
83 M. Arif, M. A. Raja, S. Zeenat, Z. Chi and C. Liu, *J. Biomater. Sci., Polym. Ed.*, 2017, **28**, 50–62.
84 A. Guzmán Rodríguez, M. Sablón Carrazana, C. Rodríguez Tanty, M. J. Malessy, G. Fuentes and L. J. Cruz, *Cancers*, 2022, **15**, 4.
85 M.-R. Ozturk, M. Popa, D. M. Rata, A. N. Cadinoiu, F. Parfait, C. Delaite, L. I. Atanase, C. Solcan and O. M. Daraba, *Int. J. Mol. Sci.*, 2022, **23**, 9382.
86 R. Antony, S. T. David, K. Karuppasamy, G. Sanjeev and S. Balakumar, *Spectrochim. Acta, Part A*, 2014, **124**, 178–186.
87 M. Pandey, H. Choudhury, T. A. Gunasegaran, S. S. Nathan, S. Md, B. Gorain, M. Tripathy and Z. Hussain, *Drug Delivery Transl. Res.*, 2019, **9**, 520–533.
88 H. H. Abduljabbar and S. N. Abd Alhammid, *Asian J. Pharm. Clin. Res.*, 2019, **12**, 216–221.
89 R. Maji, N. S. Dey, B. S. Satapathy, B. Mukherjee and S. Mondal, *Int. J. Nanomed.*, 2014, **9**, 3107.
90 N. Ravikumara, M. Bharadwaj and B. Madhusudhan, *J. Biomater. Appl.*, 2016, **31**, 755–772.
91 M. A. Altamimi and S. H. Neau, *Saudi Pharm. J.*, 2017, **25**, 419–439.
92 K. Vijayalakshmi, B. Devi, P. Sudha, J. Venkatesan and S. Anil, *J. Nanomed. Nanotechnol.*, 2016, **7**, 419.
93 S. S. Gupta, A. Meena, T. Parikh and A. T. Serajuddin, *J. Excipients Food Chem.*, 2016, **5**, 32–45.
94 M. T. Chevalier, N. Rescignano, S. Martin-Saldaña, Á. González-Gómez, J. M. Kenny, J. San Román, C. Mijangos and V. A. Álvarez, *Eur. Polym. J.*, 2017, **95**, 348–357.
95 Y. Dai, X. Chen and X. Zhang, *Polym. Chem.*, 2019, **10**, 34–44.
96 S. A. Abouelmagd, N. H. Abd Ellah and B. N. Abd El Hamid, in *Stimuli Responsive Polymeric Nanocarriers for Drug Delivery Applications*, Elsevier, 2019, pp. 87–109.
97 M. Imran and M. R. Shah, in *Design and Development of New Nanocarriers*, Elsevier, 2018, pp. 365–400.
98 H. Wen, Y. Yin, C. Huang, W. Pan and D. Liang, *Sci. China: Chem.*, 2017, **60**, 130–135.